Historical and future changes in air pollutants from CMIP6 models

Steven T. Turnock[1], Robert J. Allen[2], Martin Andrews[1], Susanne E. Bauer[3,4], Louisa Emmons[5], Peter Good[1], Larry Horowitz[6], Martine Michou[7], Pierre Nabat[7], Vaishali Naik[6], David Neubauer[8], Fiona M. O'Connor[1], Dirk Olivié[9], Michael Schulz[9], Alistair Sellar[1], Toshihiko Takemura[10], Simone Tilmes[5], Kostas Tsigaridis[3,4], Tongwen Wu[11], Jie Zhang[11]

[1]Met Office Hadley Centre, Exeter, UK
[2]Department of Earth and Planetary Sciences, University of California Riverside, Riverside, California, USA
[3]Center for Climate Systems Research, Columbia University, New York, NY, USA
[4]NASA Goddard Institute for Space Studies, New York, NY, USA
[5]Atmospheric Chemistry Observations and Modelling Lab, National Center for Atmospheric Research, Boulder, CO, USA
[6]DOC/NOAA/OAR/Geophysical Fluid Dynamics Laboratory. Biogeochemistry, Atmospheric Chemistry, and Ecology Division, Princeton, USA
[7]Centre National de Recherches Météorologiques (CNRM), Université de Toulouse, Météo-France, CNRS, Toulouse, France
[8]Institute of Atmospheric and Climate Science, ETH Zurich, Zurich, Switzerland
[9]Division for Climate Modelling and Air Pollution, Norwegian Meteorological Institute, Oslo, Norway
[10]Research Institute for Applied Mechanics, Kyushu University, Fukuoka, Japan
[11]Beijing Climate Center, China Meteorological Administration, Beijing, China

Correspondence to: Steven Turnock (steven.turnock@metoffice.gov.uk)

Supplementary Material

Contents

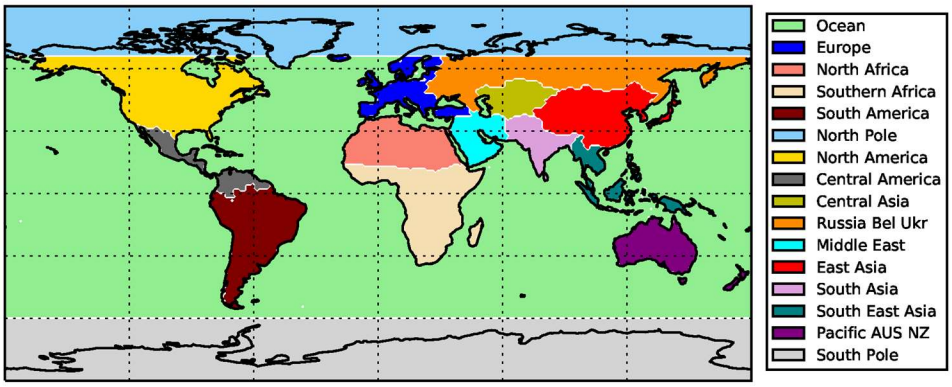

Figure S1 – Definition of regions used in the study, based on those used in Phase 2 of the Hemispheric Transport of Air Pollutants (HTAP2)

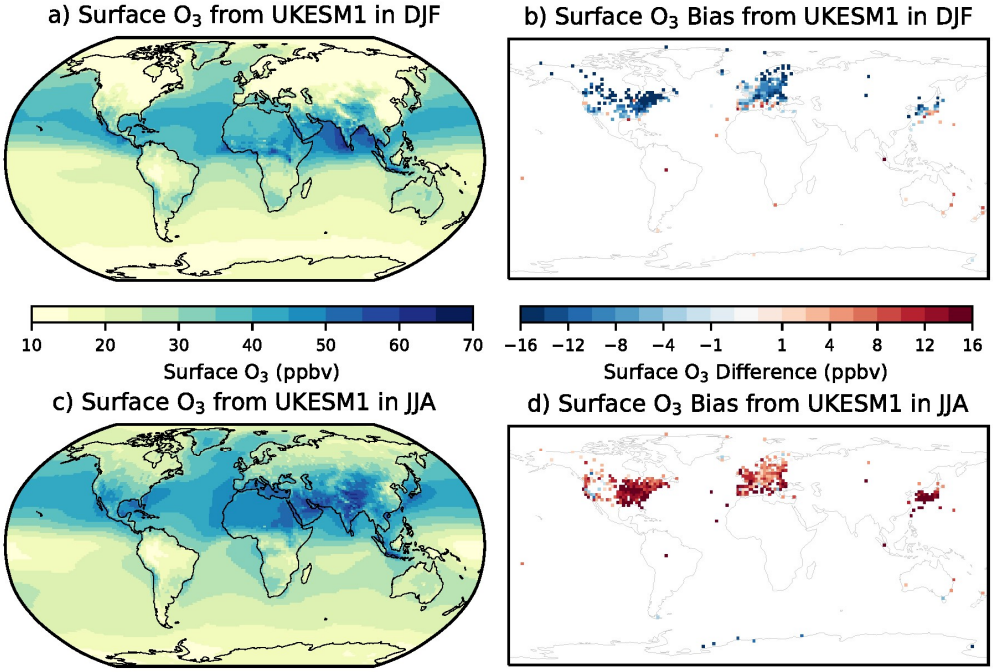

Figure S2 – Seasonal mean surface O_3 concentrations from UKESM1 in a) December January, February (DJF) and c) June, July, August (JJA) over the 2005-2014 period. Difference between the UKESM1 mean and TOAR observations for b) DJF and d) JJA.

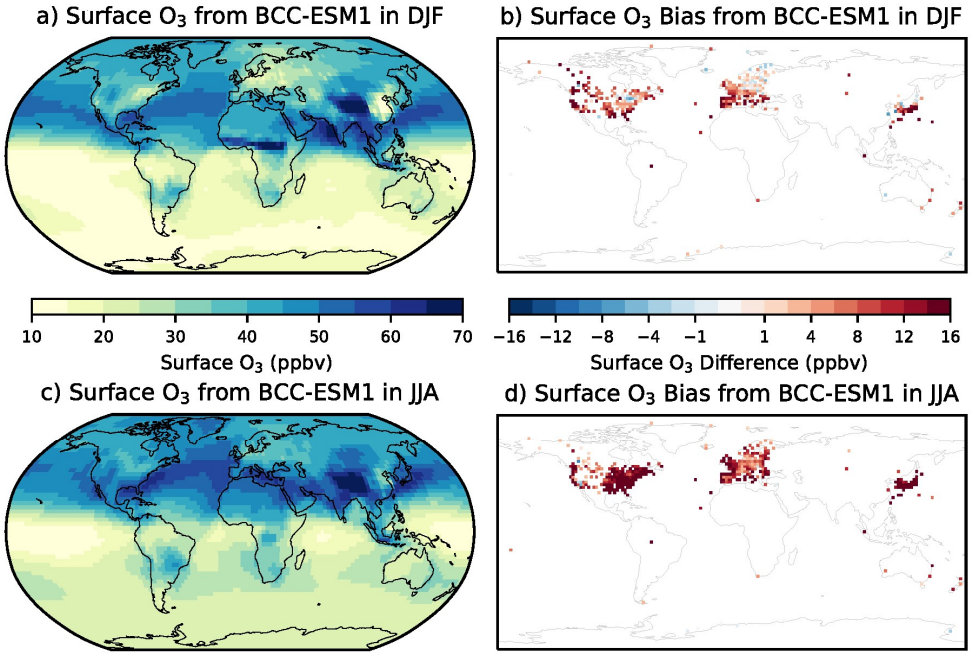

Figure S3 – Seasonal mean surface O_3 concentrations from BCC-ESM1 in a) December January, February (DJF) and c) June, July, August (JJA) over the 2005-2014 period. Difference between the BCC-ESM1 mean and TOAR observations for b) DJF and d) JJA.

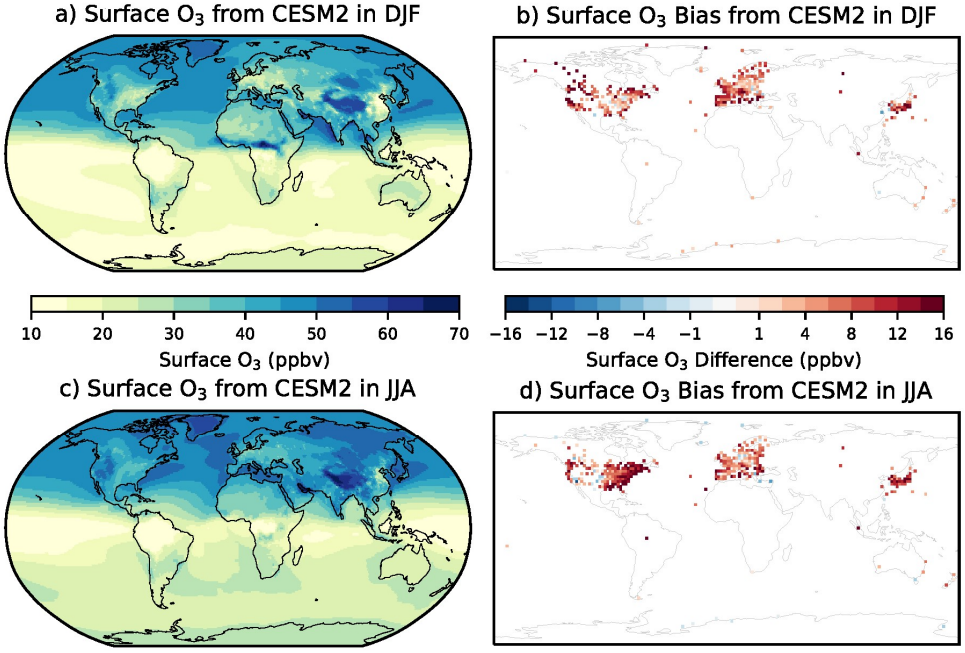

Figure S4 – Seasonal mean surface O_3 concentrations from CESM2 in a) December January, February (DJF) and c) June, July, August (JJA) over the 2005-2014 period. Difference between the CESM2 mean and TOAR observations for b) DJF and d) JJA.

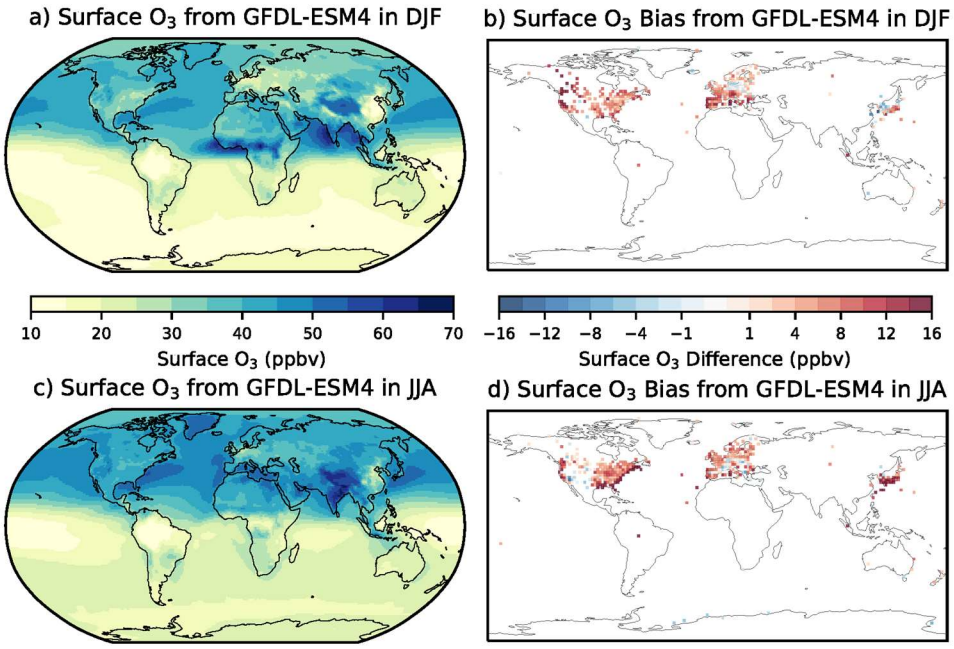

Figure S5 – Seasonal mean surface O_3 concentrations from GFDL-ESM4 in a) December January, February (DJF) and c) June, July, August (JJA) over the 2005-2014 period. Difference between the GFDL-ESM4 mean and TOAR observations for b) DJF and d) JJA.

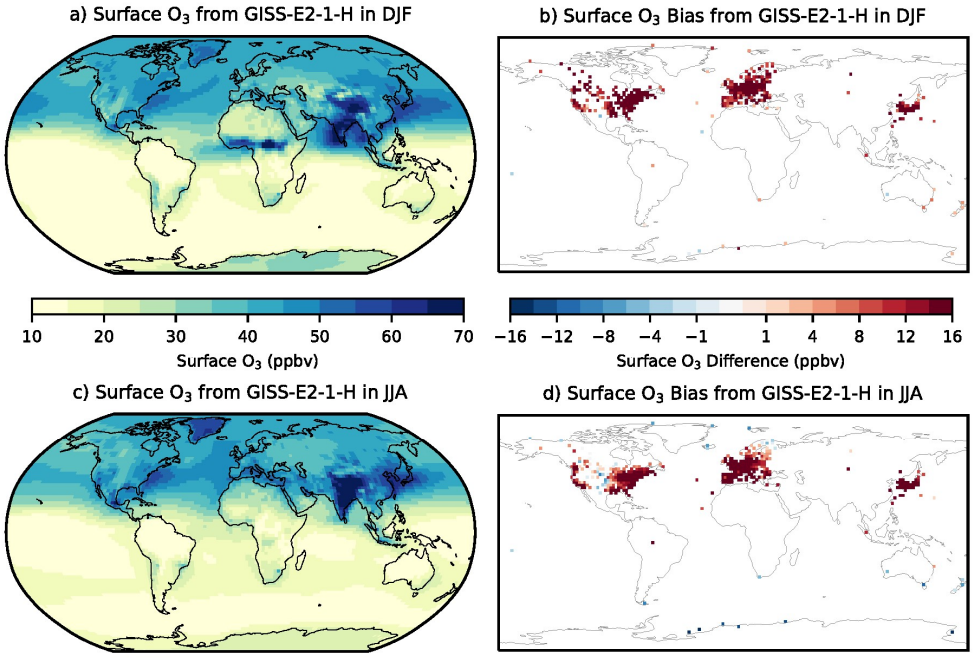

Figure S6 – Seasonal mean surface O_3 concentrations from GISS-E2-1-H in a) December January, February (DJF) and c) June, July, August (JJA) over the 2005-2014 period. Difference between the GISS-E2-1-H mean and TOAR observations for b) DJF and d) JJA.

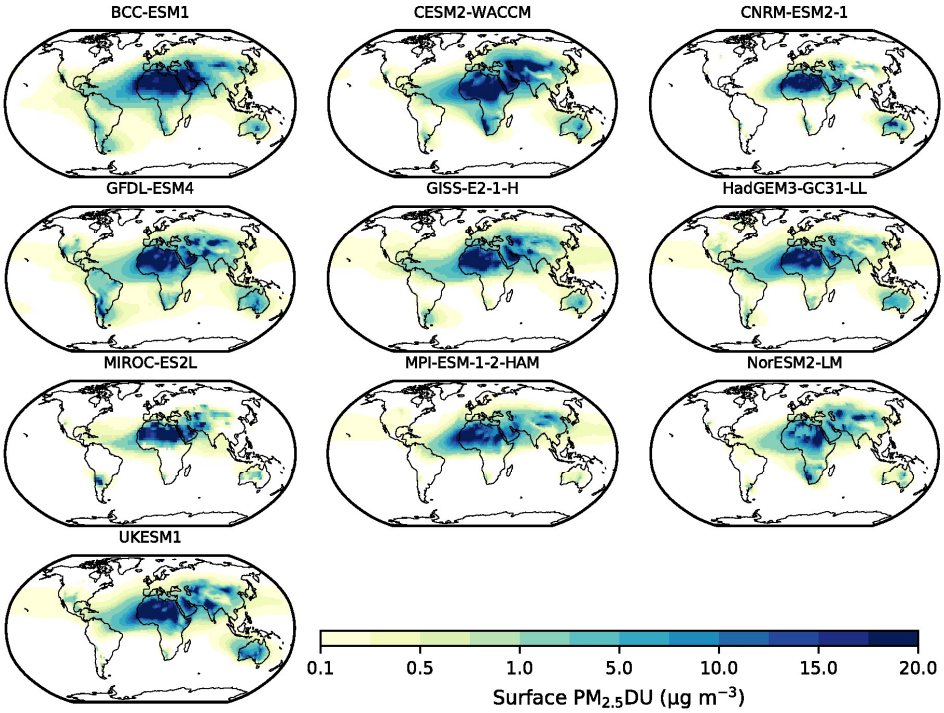

Figure S7 – Annual mean $PM_{2.5}$ dust component calculated for each individual CMIP6 model over the period 2005-2014

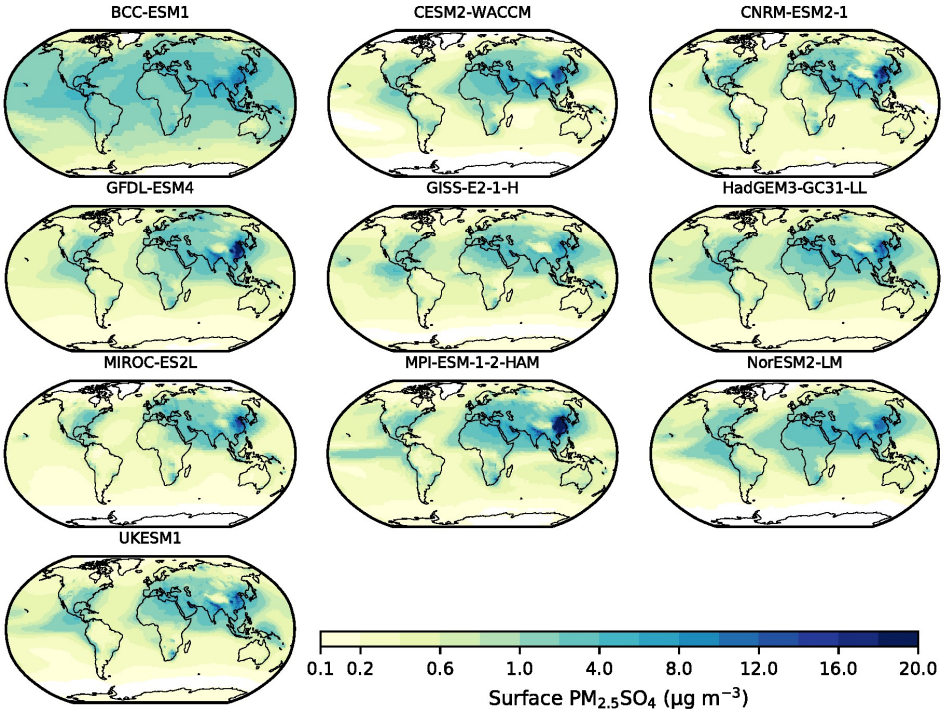

Figure S8 – Annual mean $PM_{2.5}$ SO4 component calculated for each individual CMIP6 model over the period 2005-2014

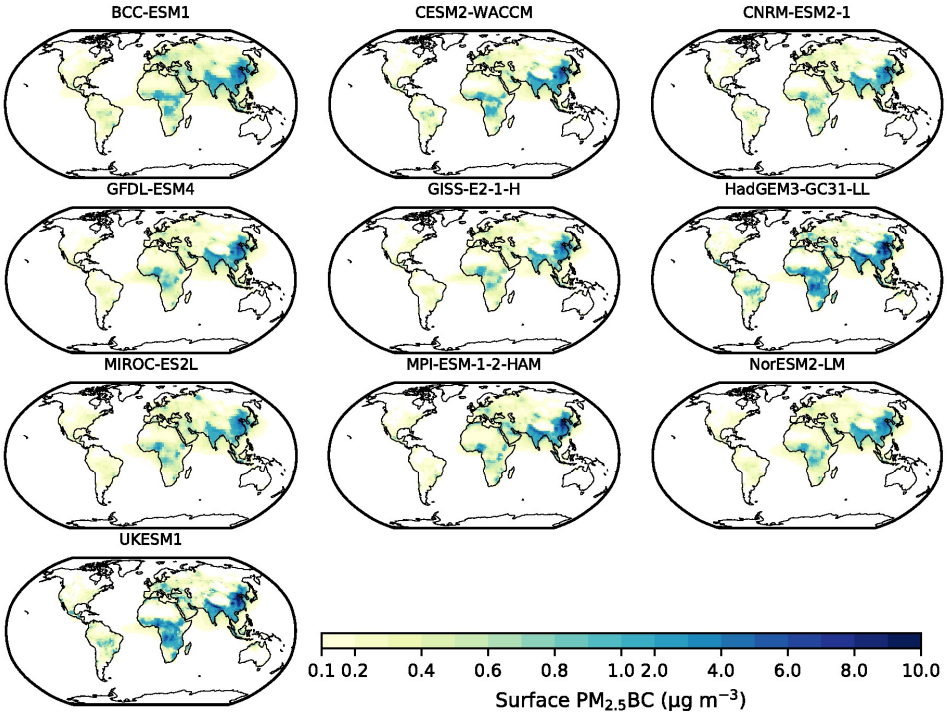

Figure S9 – Annual mean $PM_{2.5}$ BC component calculated for each individual CMIP6 model over the period 2005-2014

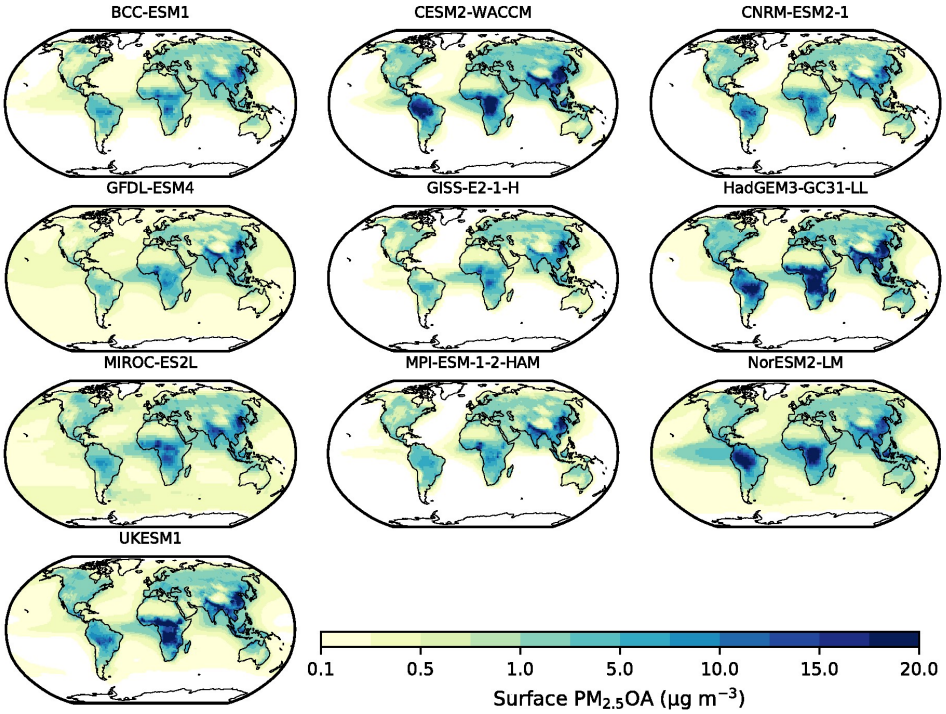

Figure S10 – Annual mean $PM_{2.5}$ OA component calculated for each individual CMIP6 model over the period 2005-2014

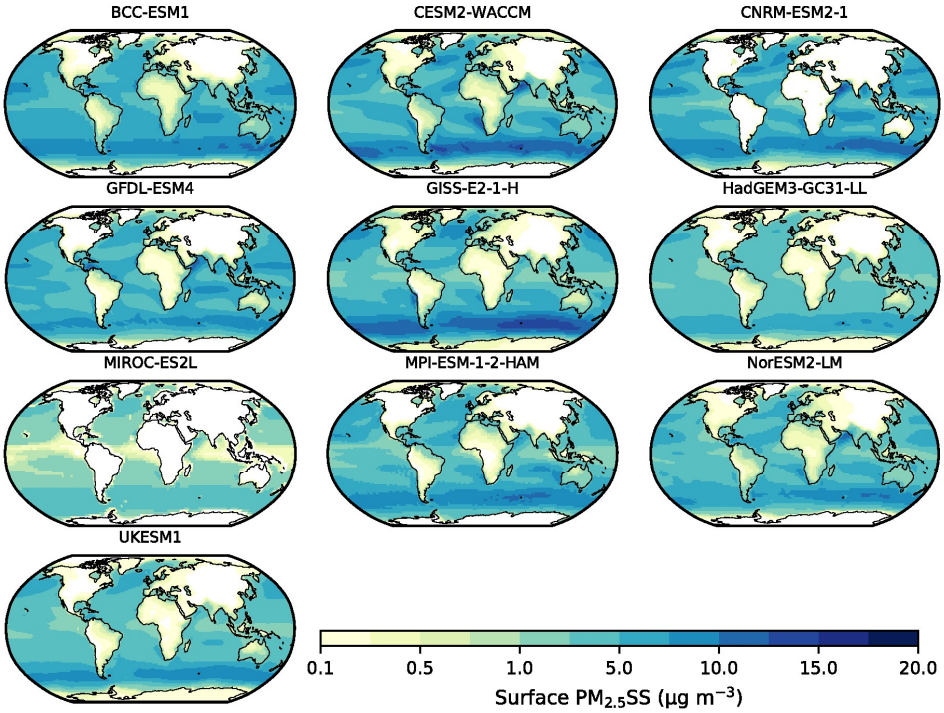

Figure S11 – Annual mean $PM_{2.5}$ SS component calculated for each individual CMIP6 model over the period 2005-2014

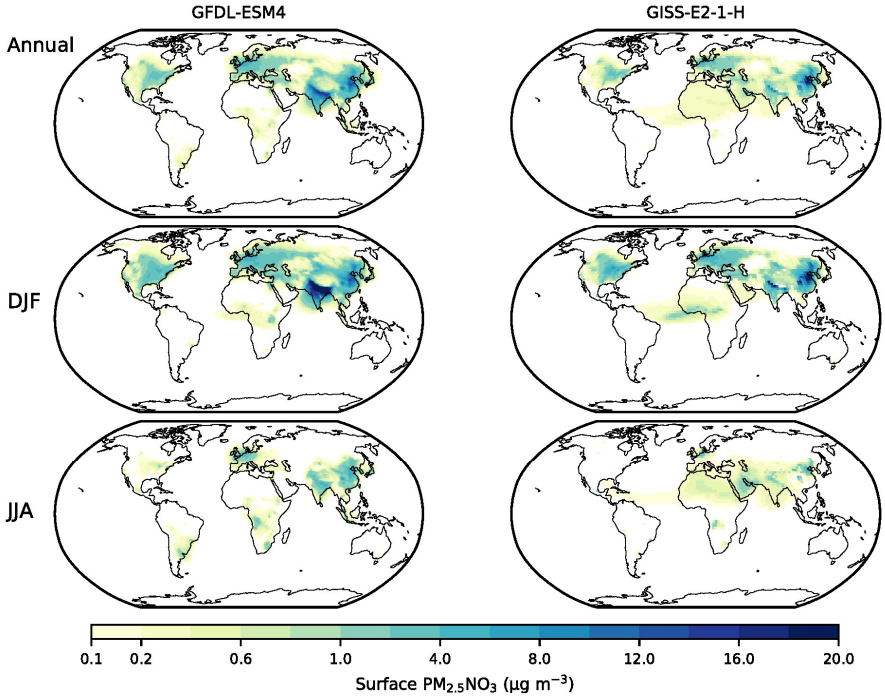

Figure S12 – Annual and seasonal mean $PM_{2.5}$ NO_3 (nitrate) component calculated for each individual CMIP6 model that made the data available over the period 2005-2014

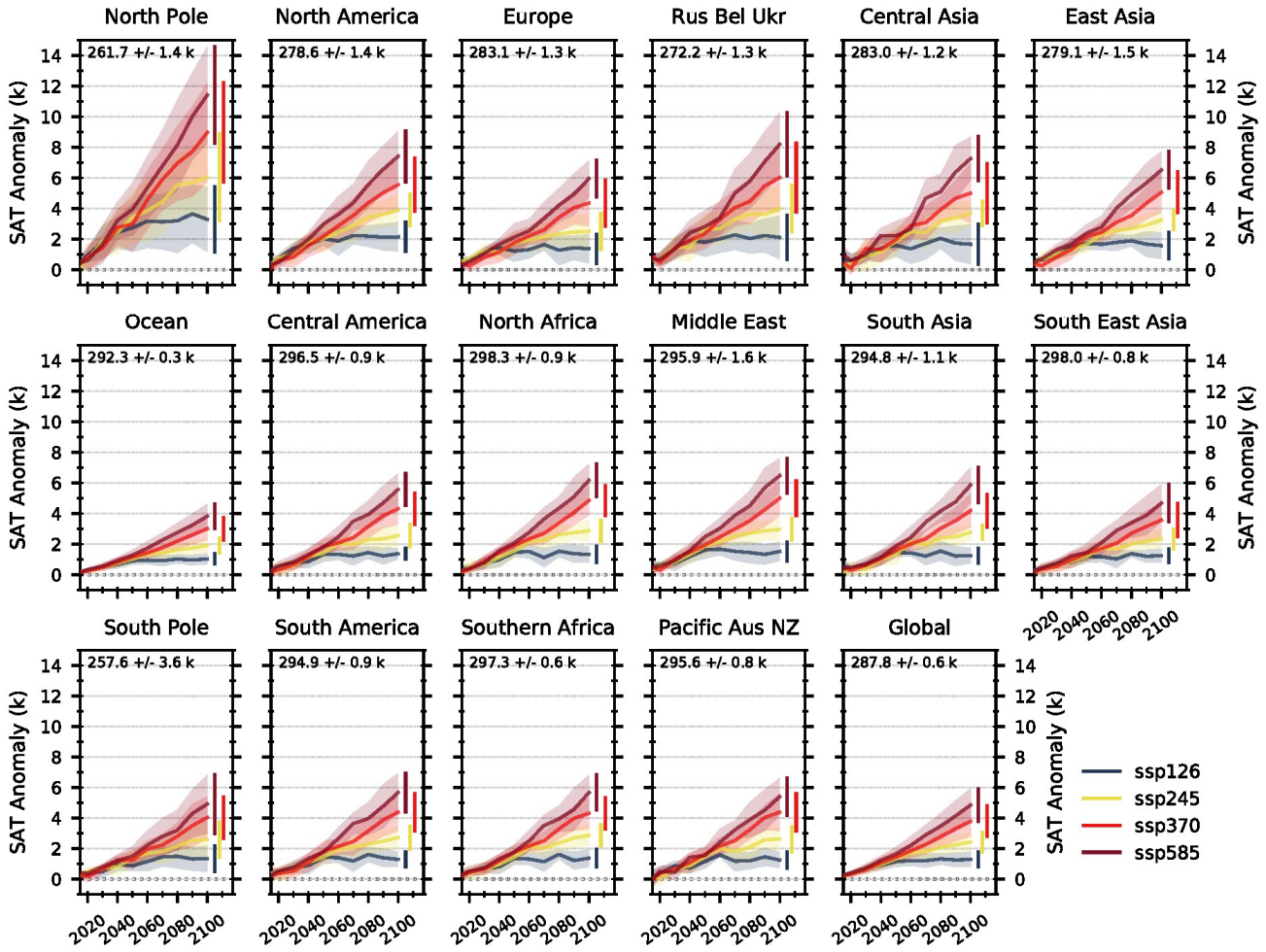

Figure S13 – Regional surface air temperature response across 5 CMIP6 models (CESM2-WACCM, CNRM-ESM2-1, GFDL-ESM4, MIROC-ES2L and UKESM1) for the Tier 1 future scenarios. Each line represents a multi-model mean across the region with shading representing the +/- 1 standard deviation in the mean. The multi-model regional mean value (+/- 1 standard deviation) for the year 2005-2014 is shown in the top left corner of each panel.

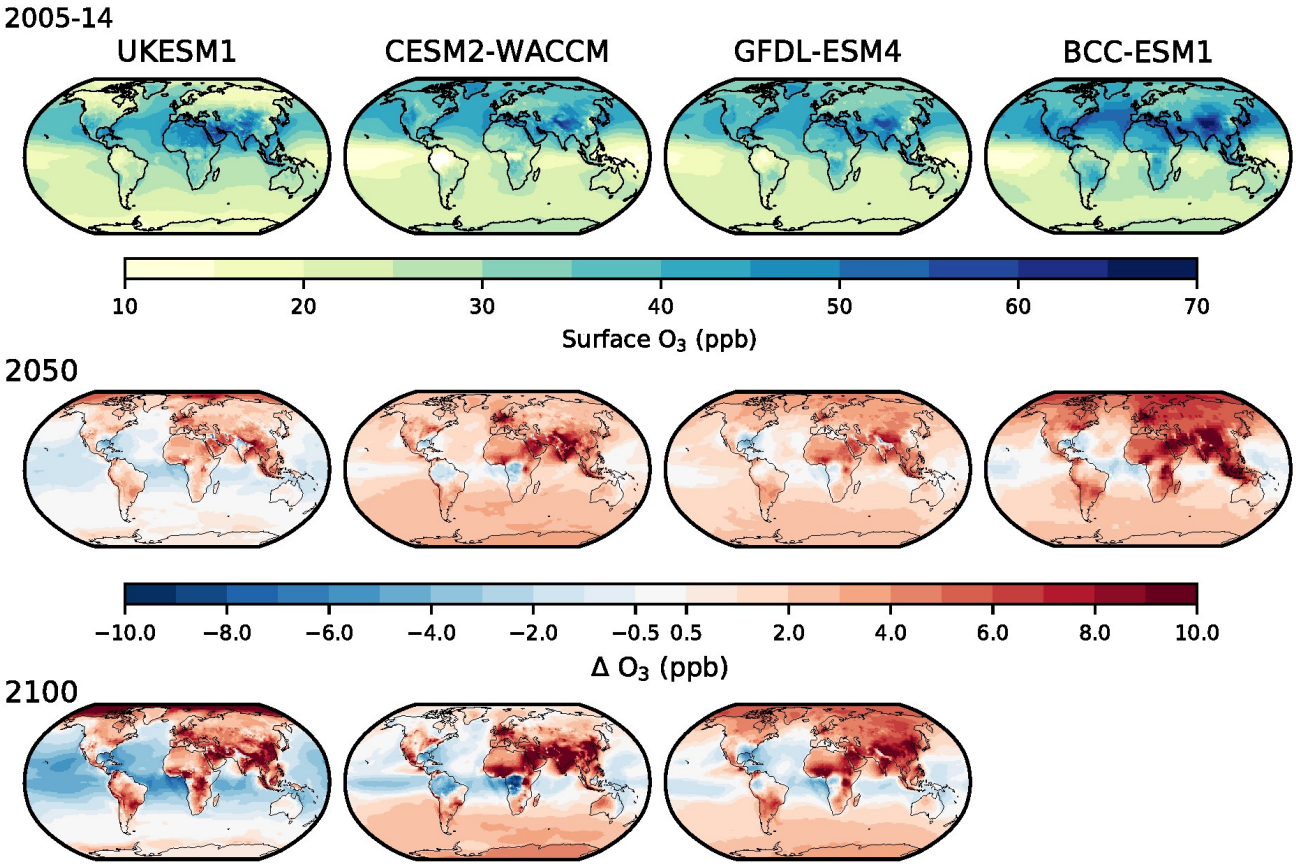

Figure S14 – Annual mean surface O_3 concentrations and future response in ssp370 across four different CMIP6 models. Top row shows the 2005-2014 annual mean surface O_3 concentrations in each model from the historical simulations. Middle row shows the surface O_3 response in 2050, relative to 2005-2014 mean, in each model for ssp370. Bottom row shows the same as the middle but for 2100. No data is presented in 2100 for BCC-ESM1 as data for ssp370 only extended out to 2055.

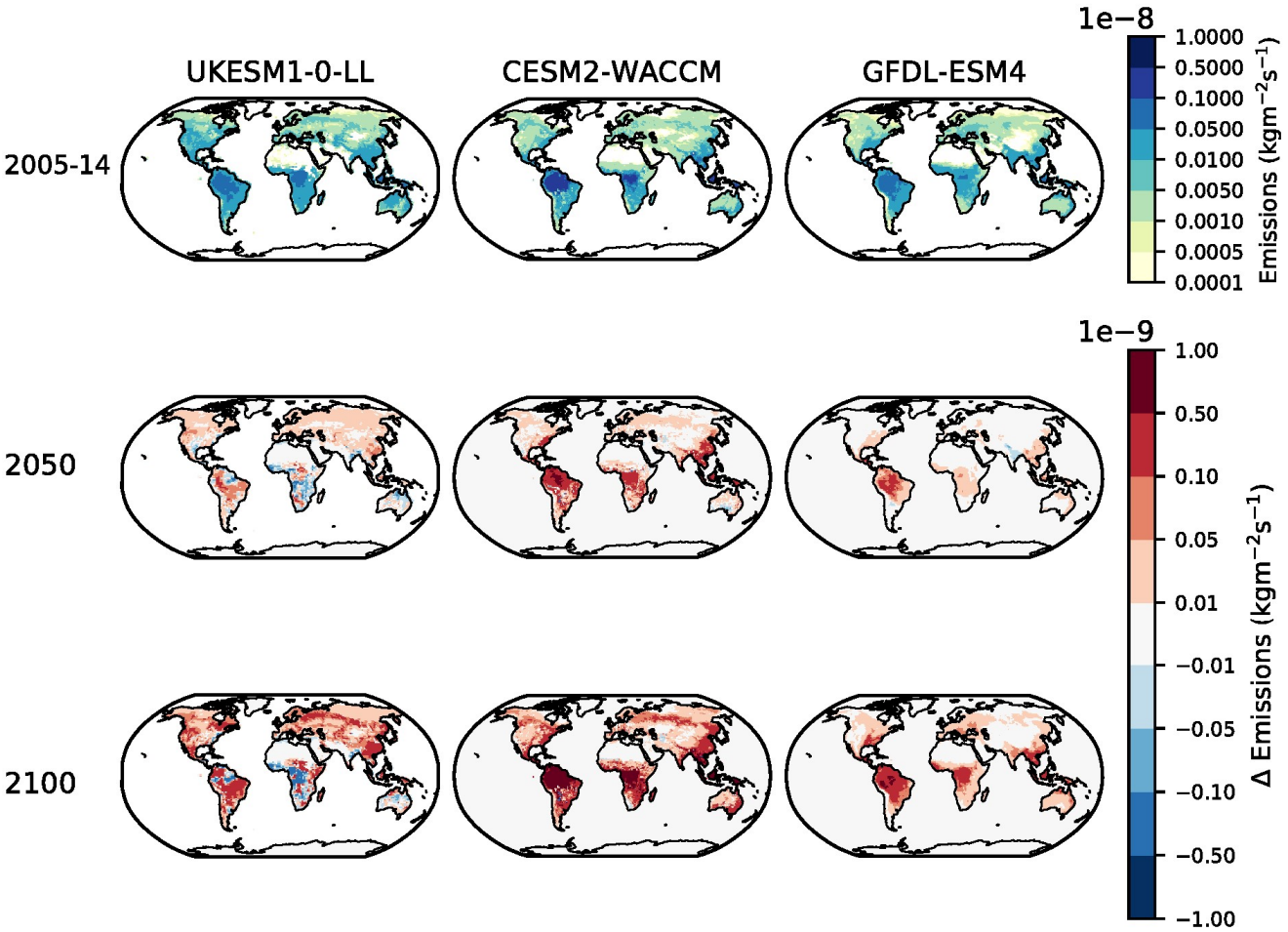

Figure S15 – Annual mean emissions of total biogenic volatile organic compounds across CMIP6 models. Top row shows the 2005-2014 annual mean emissions in each model from the historical simulations. Middle row shows 2050 change in emissions, relative to 2005-2014 mean, in each model for ssp370. Bottom row shows the same as the middle but for 2100.

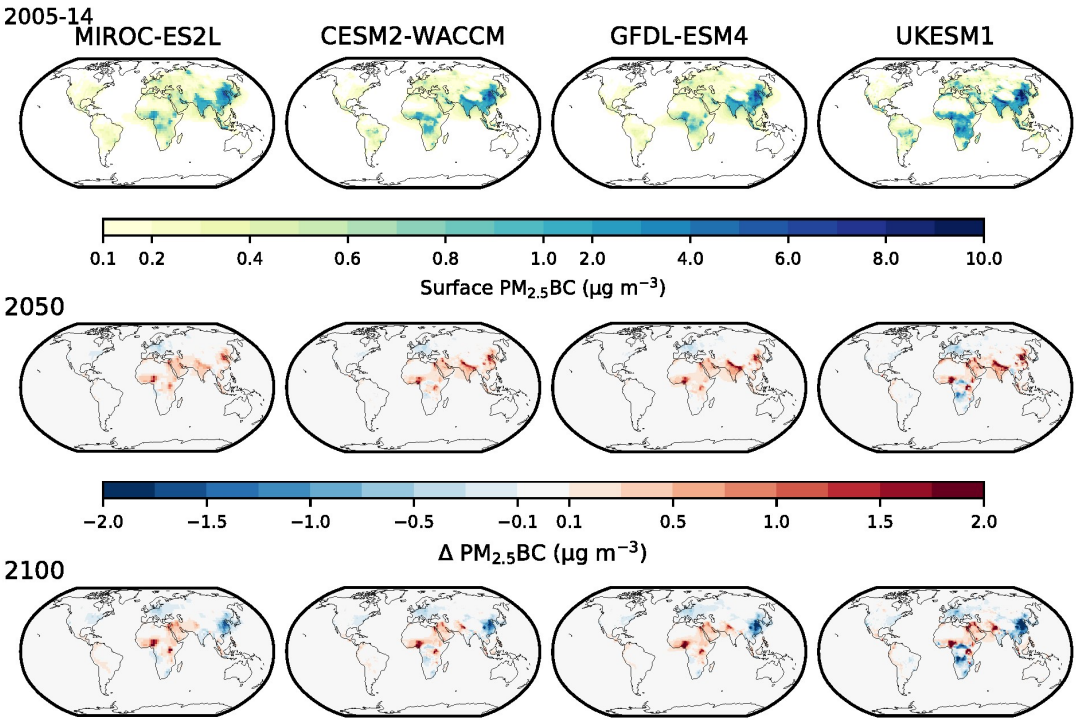

Figure S16 – Annual mean surface $PM_{2.5}$ black carbon concentrations and future response in ssp370 across four different CMIP6 models. Top row shows the 2005-2014 annual mean surface $PM_{2.5}$ black carbon concentrations in each model from the historical simulations. Middle row shows the decadal mean surface $PM_{2.5}$ black carbon response in 2050 (2045-2055), relative to 2005-2014 mean, in each model for ssp370. Bottom row shows the same as the middle but for 2095 (2090-2100).

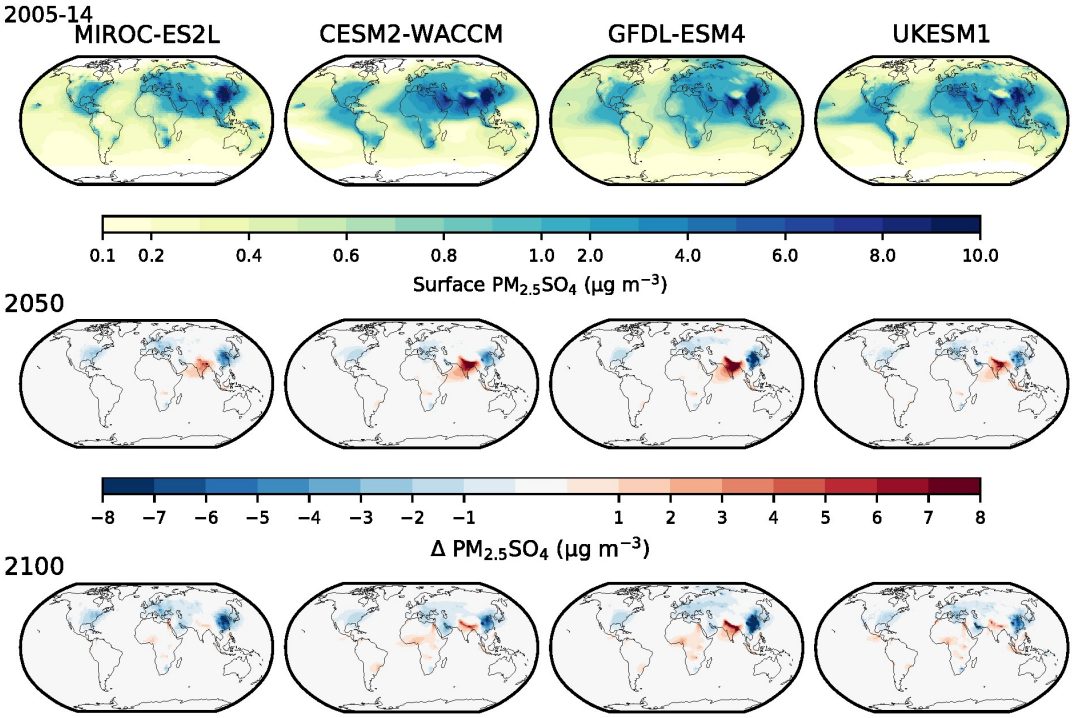

Figure S17 – same as Fig S16 but for $PM_{2.5}$ sulphate

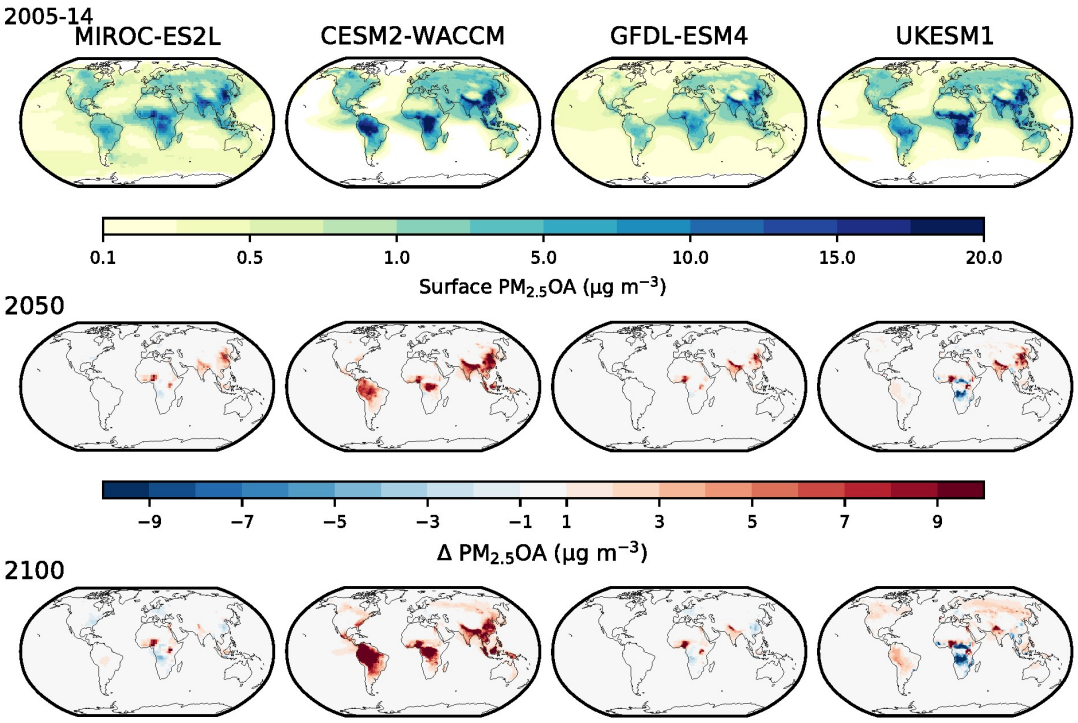

Figure S18 – same as Fig S16 but for $PM_{2.5}$ organic aerosol

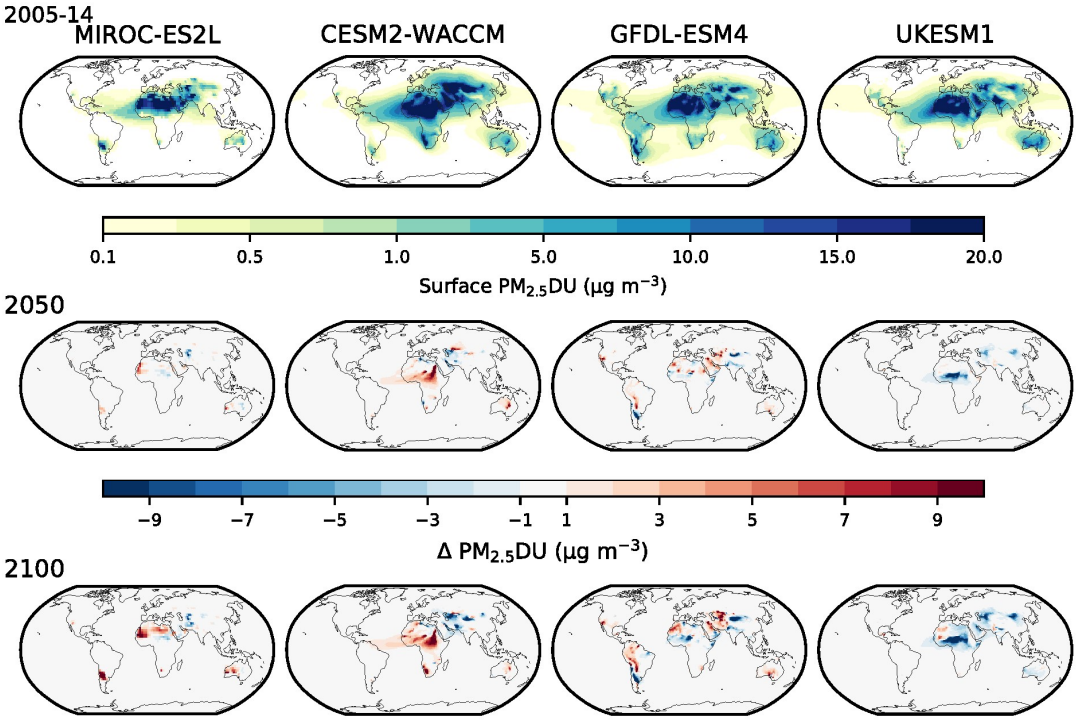

Figure S19 – same as Fig S16 but for $PM_{2.5}$ dust

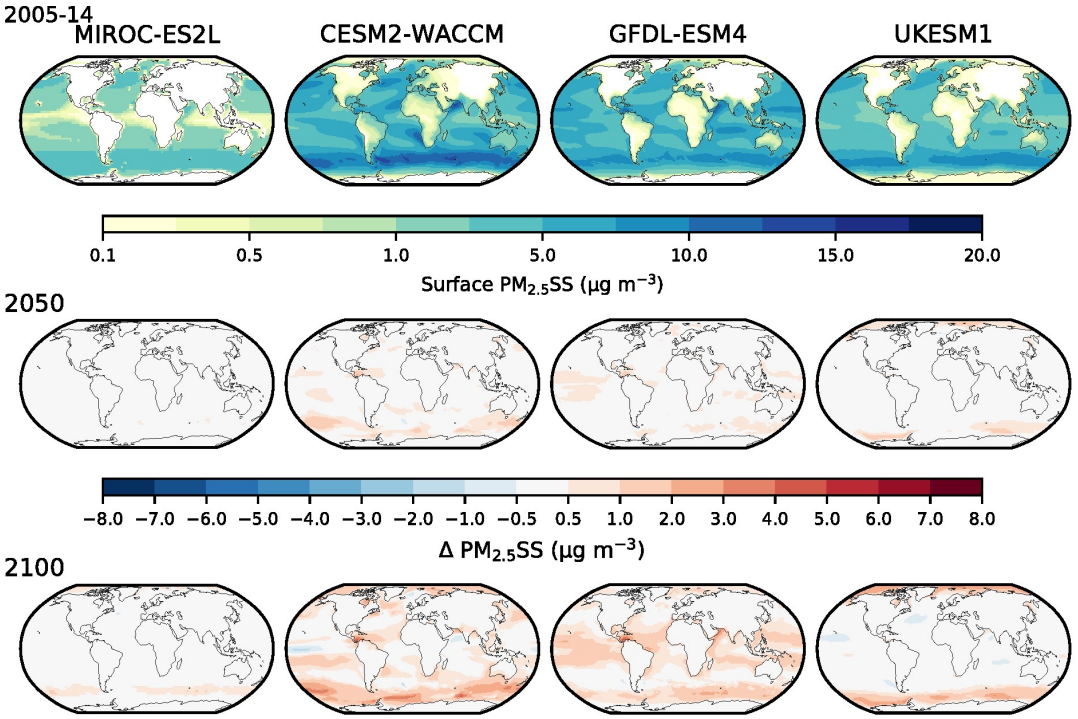

Figure S20 – same as Fig S16 but for $PM_{2.5}$ sea salt